

Renhe Shi

School of Aerospace Engineering,
Beijing Institute of Technology,
Beijing 100081, China
e-mail: shirenhe@bit.edu.cn

Li Liu

School of Aerospace Engineering,
Beijing Institute of Technology,
Beijing 100081, China;
Key Laboratory of Dynamics and Control of Flight
Vehicle,
Ministry of Education,
Beijing 100081, China
e-mail: liuli@bit.edu.cn

Teng Long

School of Aerospace Engineering,
Beijing Institute of Technology,
Beijing 100081, China;
Key Laboratory of Dynamics and Control of Flight
Vehicle,
Ministry of Education,
Beijing 100081, China
e-mails: tenglong@bit.edu.cn; bitryu@gmail.com

Yufei Wu

School of Aerospace Engineering,
Beijing Institute of Technology,
Beijing 100081, China
e-mail: wuyufei@bit.edu.cn

G. Gary Wang

School of Mechatronic Engineering System,
Simon Fraser University,
Surrey V3T 0A3, Canada
e-mail: gary_wang@sfu.ca

Multi-Fidelity Modeling and Adaptive Co-Kriging-Based Optimization for All-Electric Geostationary Orbit Satellite Systems

All-electric geostationary orbit (GEO) satellite systems design is a challenging multidisciplinary design optimization (MDO) problem, which is computation-intensive due to the employment of expensive simulations. In this paper, the all-electric GEO satellite MDO problem with multi-fidelity models is investigated. The MDO problem involving six inter-coupled disciplines is formulated to minimize the total mass of the satellite system subject to a number of engineering constraints. To reduce the computational cost of the multidisciplinary analysis (MDA) process, multi-fidelity transfer dynamics models and finite element analysis (FEA) models are developed for the geosynchronous transfer orbit (GTO) and structure disciplines, respectively. To effectively solve the all-electric GEO satellite MDO problem using multi-fidelity models, an adaptive Co-Kriging-based optimization framework is proposed. In this framework, the samples from a high-fidelity MDA process are integrated with those from a low-fidelity MDA process to create a Co-Kriging metamodel with a moderate computational cost for optimization. Besides, for refining the Co-Kriging metamodels, a multi-objective adaptive infill sampling approach is developed to produce the infill sample points in terms of the expected improvement (EI) and the probability of feasibility (PF) functions. Optimization results show that the proposed optimization framework can significantly reduce the total mass of satellite system with a limited computational budget, which demonstrates the effectiveness and practicality of the multi-fidelity modeling and adaptive Co-Kriging-based optimization framework for all-electric GEO satellite systems design. [DOI: 10.1115/1.4044321]

Keywords: multi-fidelity optimization, multidisciplinary design optimization, Co-Kriging, all-electric GEO satellite, metamodel-based design and optimization

1 Introduction

1.1 Research Background. Satellites working in geostationary orbit (GEO) have been developed in the past decades and received growing interests due to their merits in Earth observation, navigation, and communication. In recent years, several all-electric GEO satellites have been successfully developed, such as ABS-3A and Eutelsat-115B, based on Boeing BSS-702SP platform [1], which is a remarkable development for the satellite industry. State-of-the-art all-electric GEO satellites are capable of using high-efficiency electric propulsion (EP) system to implement all transfer and maneuvers such as orbit raising, station-keeping, and attitude control (AC). Owing to the high-specific impulse of EP systems, all-electric GEO satellites are able to save considerable propellant compared with the conventional chemical ones, which significantly decreases the entire mass of the satellite system and the launch cost. Nevertheless, the transfer time to GEO is extremely prolonged (i.e., several months) caused by the low thrust of EP systems (i.e., hundreds of mN), which delays the deployment of satellites in GEO [2]. Besides, the prolonged transfer time within the Van Allen belts can result in serious radiation damage of devices on the satellite, e.g., the degradation of solar arrays, which influences the performance of the entire satellite system [3]. In view of the characteristics of EP system (i.e., low thrust and high power usage), the design of all-

electric GEO satellite systems requires specific considerations on the low-thrust orbital transfer and station-keeping maneuvers, attitude control, thermal control, power subsystem, structure configuration, etc., which naturally is a complex multidisciplinary design optimization (MDO) problem in practices.

1.2 Metamodel-Based Design Optimization. The methodology of MDO was defined as “a methodology for the design of complex engineering systems and subsystems that coherently exploits the synergy of mutually interacting phenomena” [4]. In recent years, a number of MDO methods have been developed and employed for aerospace system design [5–7]. The MDO problem of all-electric GEO satellite systems was first investigated in Ref. [8], which demonstrates the feasibility and effectiveness of MDO methods for all-electric GEO satellite systems design. Besides, high-fidelity (HF) simulation models (e.g., finite element analysis (FEA)) have been widely utilized for MDO nowadays to further improve the accuracy and reliability of the design. Although the design quality of the aerospace system can be improved by using the expensive simulation models, the massive function calls on those expensive models also result in the great computational cost of optimization. Such a high cost may even make the MDO inapplicable when faced with a limited computational budget in practices.

To reduce the computational cost of expensive simulation-based optimization problems, metamodel-based design and optimization (MBDO) methods have been widely employed in engineering

Contributed by the Design Automation Committee of ASME for publication in the JOURNAL OF MECHANICAL DESIGN. Manuscript received June 3, 2018; final manuscript received June 14, 2019; published online July 24, 2019. Assoc. Editor: Xiaoping Du.

applications [9–11]. In MBDO, a metamodel is constructed based on a set of sample points to represent the expensive simulation models or the multidisciplinary analysis (MDA) process for optimization. Based on certain infill criteria or sampling strategies, the metamodel can be adaptively refined or updated during the optimization, which leads the search to the optimum efficiently. For instance, the well-known efficient global optimization (EGO) algorithm [12] applies the Kriging metamodel for optimization, where the Kriging metamodel is gradually refined via sampling guided by the expected improvement (EI) criterion. In the literature, many MBDO methods have been developed to solve high-dimensional expensive black-box optimization problems with constraints [13–15]. And MBDO methods have also been successfully applied for aerospace system design, e.g., satellite truss optimization [16] and observation satellite system design [17]. The authors also solved an all-electric GEO satellite MDO problem by an adaptive response surface-based optimization method [8], which shows the merits of MBDO methods for solving novel spacecraft system design problems.

1.3 Multi-Fidelity Optimization. The real-world satellite system design generally involves simulation models with different levels of fidelity (e.g., the FEA model with coarse and fine grids). The HF models are more accurate but expensive, which are generally unsuitable for optimization when the computational budget is limited. On the contrary, the low-fidelity (LF) models are cheap to be evaluated, while the analysis accuracy is relatively poor. To guarantee the design quality and reduce the computational cost simultaneously, it is beneficial to utilize both the HF and LF models for optimization. However, the samples of conventional MBDO methods purely arise from the expensive HF models, which faces the challenging computational expenses due to the fact that a large number of expensive simulations or MDA processes are required to build an acceptable metamodel (e.g., more than thousands of samples for high-dimensional problems). In case of the HF and LF models in engineering practices, how to effectively organize and utilize those variable fidelity models for optimization becomes a critical issue for the designers. To address the issue, multi-model fusion or multi-fidelity methods [18] have been developed to further release the computational burden of MBDO. In multi-fidelity methods, limited expensive HF samples are integrated with a number of cheap LF samples to improve the metamodeling accuracy and optimization efficiency. Owing to the moderate computational cost and desirable accuracy, multi-fidelity MBDO methods become attractive in recent years [19–21], and many multi-fidelity optimization algorithms and their engineering applications have been reported in literatures. For instances, Chen et al. [18] developed an improved pre-posterior analysis to evaluate the multiple simulation models, in which the infill sample points are generated by a novel objective-oriented sampling criterion. Ye et al. [22] presented a Co-Kriging-based space reduction method for solving large-scale high-voltage devices design optimization problems, which finally obtained the optimal design within a reasonable time. A Bayesian surrogate modeling based multi-fidelity optimization approach was reported by Xiong et al. [23], where the objective-oriented sequential sampling in terms of statistical lower bounding criterion is used to improve the objective. However, most existing multi-fidelity methods are limited to the bounded constrained optimizations. They are mostly ineffective or even inapplicable for solving those challenging problems with constraints arising from expensive black-box simulations, such as the all-electric GEO satellite MDO problem in this study.

1.4 Contributions and Novelty. To solve the all-electric GEO satellite MDO problem, it is valuable to apply multi-fidelity methods to improve the overall design quality and save computational cost. However, two challenges need to be addressed, i.e., effective multi-fidelity modeling of the satellite system, and an efficient multi-fidelity optimization framework. In this paper, an all-

electric GEO satellite MDO problem with multi-fidelity models is defined and investigated to address the challenges above. Different from Ref. [8], the multi-fidelity models of low-thrust orbit transfer and adjoined double-satellite structures are constructed in view of the unique features of the all-electric GEO satellite system in this study. Since no research work on all-electric GEO satellite MDO problems with multi-fidelity models has been reported yet to the authors' knowledge, the multi-fidelity modeling work in this paper is a rather new endeavor for satellite system design practices. Besides, a novel adaptive Co-Kriging-based optimization framework that can handle expensive constraints is developed to solve the all-electric GEO satellite MDO problem with multi-fidelity models. In the framework, the Co-Kriging method is employed to achieve the fusion of models with different levels of fidelity owing to the merits of the Gaussian process. And the Co-Kriging is sequentially refined by a multi-objective adaptive infill sampling approach to improve the optimality and feasibility of optimization.

The remainder of this paper is organized as follows. The studied all-electric GEO satellite multiple-fidelity MDO problem involving six disciplines is introduced in Sec. 2. The multi-fidelity models of GTO and structure disciplines are constructed in Sec. 3. In Sec. 4, the Co-Kriging method is briefly reviewed, and the adaptive Co-Kriging-based optimization framework is detailed including the optimization procedure and metamodel refining mechanism and tested on a number of numerical benchmark problems. The all-electric GEO satellite MDO problem with multi-fidelity models is solved by the proposed adaptive Co-Kriging-based optimization framework in Sec. 5, and the optimization results are discussed in detail. Finally, the conclusions and future work are given in Sec. 6.

2 All-Electric Geostationary Orbit Satellite Multi-Fidelity Multidisciplinary Design Optimization Problem

The studied all-electric GEO satellite in this work is from Ref. [8]. Four electric thrusters with a maximum thrust of 200 mN and 4000 s specific impulse are utilized to implement the orbit transfer, station-keeping, and attitude control. Compared with the conventional chemical satellite, the all-electric satellite can save enormous propellant owing to the superior efficiency of the EP system. Hence, the all-electric GEO satellites are usually launched through the “two satellites with one rocket” way (e.g., the launch of BSS-702SP satellites using Falcon-9), which significantly reduces the launch cost. However, the associated transfer time of the all-electric GEO satellite is significantly prolonged, which poses challenges for low-thrust orbital maneuver control, radiation damage protection, etc.

In view of the differences between the all-electric GEO satellite system and the conventional chemical one, the most challenging disciplines for all-electric GEO satellite system design are taken into account in the MDO problem, i.e., geosynchronous transfer orbit (GTO), GEO station-keeping, solar power, thermal control (TC), AC, and structure [8]. In the GTO discipline, a two-stage low-thrust transfer model is employed to compute the total transfer time based on Gaussian orbit dynamics. And the east/west station-keeping (EWSK) and north/south station-keeping (NSSK) accuracy is determined in the GEO station-keeping discipline, given the position of electric thrusters. In the power discipline, the area of the solar arrays and the capacity of the battery are respectively designed to provide sufficient power, where the degradation of solar cells caused by the radiation damage is considered. In the TC and AC disciplines, the area of radiators and the capability of reaction wheels are designed to guarantee the operation of satellite in orbit. For the structure discipline, the FEA model of the satellite is built to calculate the natural frequencies as the constraints of the MDO problem.

The design structure matrix (DSM) of the all-electric GEO satellite MDO problem in this work is organized in Fig. 1 to graphically

coordinate system, $w = 1 + f \cos L + g \sin L$ and $s^2 = 1 + h^2 + k^2$ are the intermediary variables. The simulation step of the dynamics in the HF model is set to be 500 s.

In the HF model, the perturbations due to the first four zonal harmonics of non-spherical gravitational potential are taken into account, which is detailed in Ref. [25].

The influence of eclipses is also considered for the HF model of GTO discipline. When the eclipses occur, the EP system cannot work because the solar arrays cannot provide power in the shadow of the Earth, which extends the transfer time. The eclipse model is graphically illustrated in Fig. 3 [8]. In the HF model, the thrust acceleration $F = 0$ if the satellite enters the umbra or penumbra according to Eq. (3) [26]

$$\begin{cases} \psi_1 < \psi < \psi_2 & \text{umbra} \\ \psi_2 \leq \psi & \text{penumbra} \end{cases} \quad (3)$$

$$\begin{cases} \psi_1 = \pi - \arcsin\left(\frac{a_e}{r}\right) - \arcsin\left(\frac{R_s + a_e}{r}\right) \\ \psi_2 = \pi - \arcsin\left(\frac{a_e}{r}\right) + \arcsin\left(\frac{R_s + a_e}{r}\right) \end{cases}$$

where ψ is the field angle for the Earth center between the satellite and sun; ψ_1 and ψ_2 are the field angles when the satellite is located on the boundaries of penumbra and umbra, respectively, $R_s = 696,000$ km is the radius of the sun.

3.1.2 Low-Fidelity Model. The LF model is also formulated by the Gaussian dynamics in terms of MEEs as shown in Eq. (2), while the simulation step is set to be 1000 s to save computational cost. Besides, the perturbations and influence of eclipses are ignored in the LF model, i.e., $a = [0, 0, 0]$, and the electric thrusters will work at the maximum thrust level during the entire transfer process.

In summary, the differences between HF and LF models of GTO discipline are presented in Table 3. To compare HF and LF models of GTO discipline, the total transfer time with respect to the yaw angle α of the first stage is exhibited in Fig. 4. The results indicate that the total transfer time is decreased with the increasing of α , and the overall trends of the HF and LF models are coincident. However, the total transfer time from the LF model is generally lower than that of the HF models due to the ignorance of the disturbance perturbations and eclipses.

3.2 Multi-Fidelity Modeling of Structure Discipline. The structural FEA model of the satellite is built to compute the first-order bending frequency of the satellites as the local constraints. The satellite structure is a cuboid consisting of a communication cabin, a service cabin with four fuel tanks inside, and a $\Phi 1200$ mm central cylinder. The structure configuration of an isolated satellite is shown in Fig. 5 [8].

3.2.1 High-Fidelity Model. Owing to the saved propellant mass, the all-electric GEO satellite is much lighter than the competitive chemical satellite. Hence, the all-electric GEO satellites are launched through the “two satellites with one rocket” way in

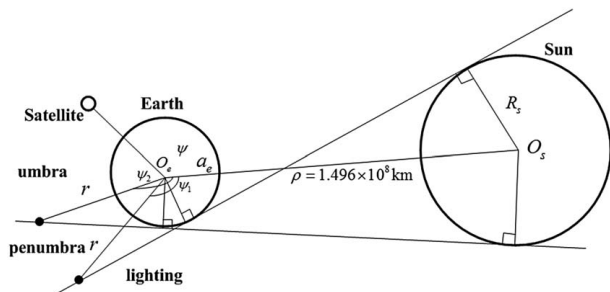


Fig. 3 Illustration of the Earth shadow model

Table 3 Differences of HF/LF models in the GTO discipline

	HF model	LF model
Simulation step	500 s	1000 s
Perturbations	Consider	Not consider
Eclipses	Consider	Not consider
Mean running time	30.0 s	9.0 s

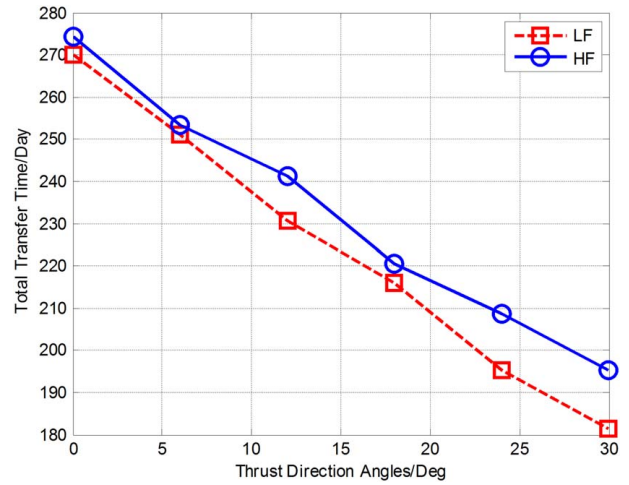


Fig. 4 Comparison of the HF/LF GTO models

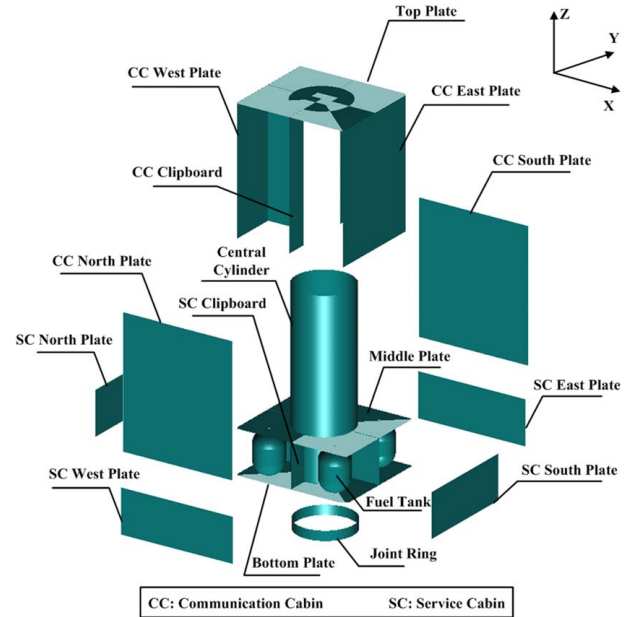


Fig. 5 Structural configuration of the satellite (SC, service cabin; CC, communication cabin)

engineering practices. In this way, the satellites are connected in a longitudinal direction within the fairing of the rocket. In the HF model of structure discipline, the FEA model of adjoined double-satellite is shown in Fig. 6, which involves 12,590 elements and 12,062 nodes. In the FEA model, the bottom plate, service cabin plates, communication cabin plates, middle plate, and top plate are made of aluminum alloy honeycomb sandwich material. The clipboards and central cylinder are made of carbon fiber-reinforced composite material to enhance the stiffness of the structure. The mass of other subsystems and propellant is modeled by nonstructural mass (NSM) or lumped mass linked to the structure and fuel

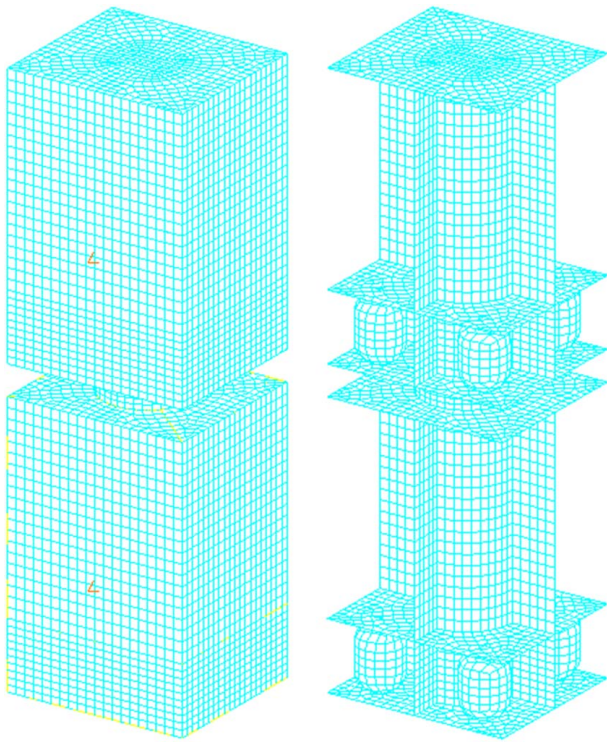


Fig. 6 High-fidelity FEA model of two adjoined satellites

tanks. Specifically, the solar arrays are modeled as the lumped mass on the south/north structural plates for modal analysis.

3.2.2 Low-Fidelity Model. In the LF model of structure discipline, the FEA model of the isolated satellite is built to estimate the natural frequencies of the adjoined double-satellite, as displayed in Fig. 7 [8]. The LF model includes 6235 elements and 5991 nodes, which is less than half of those in the HF model. The material of structural plates, clipboards, and central cylinder are the same as those in the HF model. The other system mass and solar arrays are also modeled as NSM and lumped mass in the LF model.

To estimate the frequencies of the adjoined double-satellite in practice, the satellite structure can be approximately regarded as a cantilever beam, whose first-order bending frequency f is calculated by Eq. (4)

$$f = \frac{1}{2\pi} \sqrt{\frac{EI}{mL^3}} \quad (4)$$

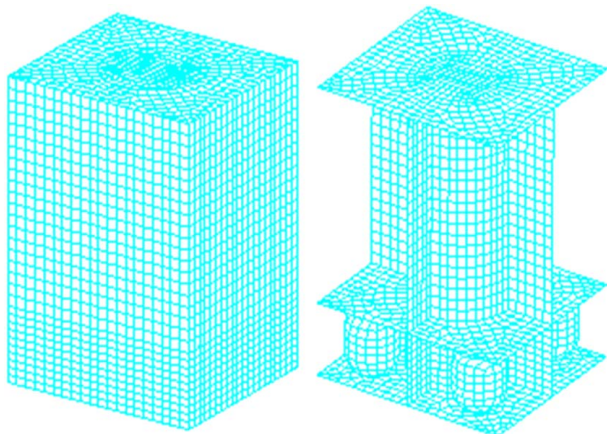


Fig. 7 Low-fidelity FEA model of an isolated satellite

Table 4 Differences of HF/LF structure models

	HF model	LF model
Number of elements	12,590	6235
Number of nodes	12,062	5991
Mean running time	79.5 s	41.2 s

where E is the Young's module, m is the mass, L is the length, and I is the moment of inertia of the cross section. When two satellites are connected together, it is assumed that the length and mass of the equivalent cantilever beam are doubled. Hence, the natural frequencies of adjoined double-satellite can be approximately estimated according to Eq. (5)

$$\tilde{f}_{LF} = \frac{1}{2\pi} \sqrt{\frac{EI}{(2m)(2L)^3}} = \frac{1}{4} \cdot \frac{1}{2\pi} \sqrt{\frac{EI}{mL^3}} = 0.25f_{LF} \quad (5)$$

where f_{LF} is the computed first-order bending frequencies from an isolated satellite FEA model, \tilde{f}_{LF} is the estimated first-order bending frequency for the adjoined double-satellite output by the LF model of the structure.

Finally, the differences between HF and LF models of structure discipline are summarized in Table 4. To make a comparison, the first-order bending frequency from the HF and LF structure discipline models are exhibited in Fig. 8, where the variable is the ply thickness of the composite. It indicates that overall trends of the HF and LF models are highly coincident, while the frequencies from the LF model are lower than that of the HF model. This is because the LF model does not consider the connection section between the two satellites, which underestimates the system stiffness.

3.3 Multidisciplinary Analysis With Multi-Fidelity Models.

In view of the feedback coupling variables in the MDO problem, an MDA process is required to obtain a compatible design during the optimization. Based on the aforementioned multi-fidelity models, the MDA process with high-fidelity GTO and structure models is termed as HF-MDA, while the MDA process with those low-fidelity models is termed as LF-MDA. The responses of objective and constraints at each sample point are obtained by evaluating the associated HF- or LF-MDA processes. In this work, a fixed-point iteration approach [8] is utilized to organize the MDA process. Given a set of design variables as defined by Table 1 in Eq. (6), the analysis results from HF- and LF-MDA processes are summarized in Table 5. Also, the mean running time of

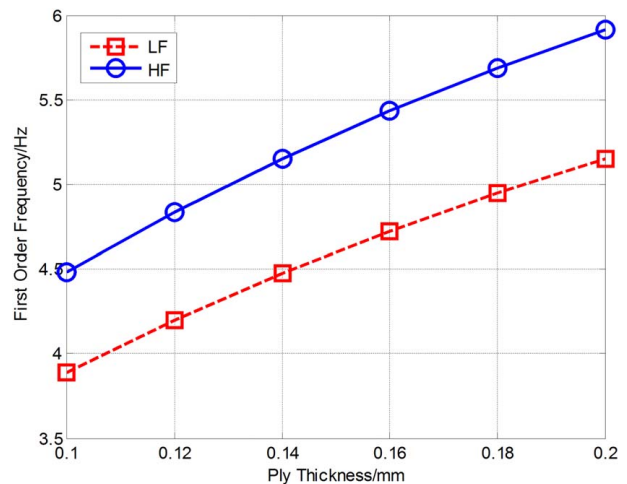


Fig. 8 Comparison of the HF/LF FEA models

Table 5 Analysis results of HF- and LF-MDA processes

Parameters	HF-MDA	LF-MDA
Total mass of satellite/kg	2656.0	2599.7
Total orbit transfer time/day	216.4	198.0
EWSK accuracy/deg	0.06	0.05
NSSK accuracy/deg	0.008	0.008
Beginning-of-life power/kW	16.70	17.51
Ending-of-life power/kW	13.51	14.18
Depth of discharge	0.74	0.74
Steady-state temperature/K	310.6	311.8
Angular momentum residue/N m s	9.21	9.25
First-order frequency round X-axis/Hz	4.91	4.31
First-order frequency round Y-axis/Hz	4.97	4.34

Table 6 Running time of HF- and LF-MDA processes

Parameters	HF-MDA	LF-MDA
CPU time/s	194.8	80.7

HF- and LF-MDA processes on a PC with Core 2 Quad CPU (2.83 GHz) and 8 GB memory is displayed in Table 6.

$$\begin{cases} \alpha = 0 \text{ deg}, \beta = 30 \text{ deg}, \varphi = 30 \text{ deg}, d_T = 900 \text{ mm}, d_N = 1050 \text{ mm}, \\ A_{sa} = 90 \text{ m}^2, C_s = 80 \text{ Ah}, A_r = 10 \text{ m}^2, \\ H_w = 50 \text{ N m s}, SH = 20 \text{ mm}, CH = 20 \text{ mm}, TBH = 25 \text{ mm}, \\ SP = 0.1 \text{ mm}, CSP = 0.1 \text{ mm}, TBP = 0.3 \text{ mm} \end{cases} \quad (6)$$

The results in Tables 5 and 6 show that most results from HF and LF-MDA processes are not identical with the relative error from 0.39% to 12.68% for different parameters. However, the computational cost of LF-MDA process is saved by more than 50% on average compared with that of HF-MDA, which significantly improves the computational efficiency for MDO.

4 Adaptive Co-Kriging-Based Optimization Framework

To effectively solve the aforementioned all-electric GEO satellite MDO problem with multi-fidelity models, a novel adaptive Co-Kriging-based optimization framework is developed as follows.

4.1 Co-Kriging Method. In this work, Co-Kriging method is used to implement the fusion of different fidelity responses from the HF-MDA and LF-MDA processes [21]. Based on the notion of correlated Gaussian process, Co-Kriging is a natural extension to Kriging, which combines cheap LF models with expensive HF models to create an inexpensive yet accurate Kriging metamodel for optimization.

To construct Co-Kriging, the LF and HF sample points are, respectively, denoted as \mathbf{X}_c and \mathbf{X}_e with $\mathbf{X}_e \subset \mathbf{X}_c$. By evaluating the expensive HF simulation model $y_e(\mathbf{x})$ and cheap LF simulation model $y_c(\mathbf{x})$, the responses at the multiple sample points are given in Eq. (7)

$$\mathbf{Y} = \begin{pmatrix} \mathbf{Y}_c(\mathbf{X}_c) \\ \mathbf{Y}_e(\mathbf{X}_e) \end{pmatrix} = [Y_c(\mathbf{x}_c^{(1)}) \dots Y_c(\mathbf{x}_c^{(n)}) \dots Y_e(\mathbf{x}_e^{(1)}) \dots Y_e(\mathbf{x}_e^{(n)}) \dots]^T \quad (7)$$

where $\mathbf{x}_c^{(n)}$ and $\mathbf{x}_e^{(n)}$ are the n th cheap and expensive sample point, respectively, $\mathbf{Y}_c(\mathbf{X}_c)$ and $\mathbf{Y}_e(\mathbf{X}_e)$ are the responses of the sample points via evaluating the cheap LF and expensive HF simulation models or MDA processes, respectively.

Co-Kriging is formulated as an integration of two Kriging metamodels with a scaling parameter ρ

$$Z_e(\mathbf{x}) = \rho Z_c(\mathbf{x}) + Z_d(\mathbf{x}) \quad (8)$$

where $Z_c(\mathbf{x})$ and $Z_e(\mathbf{x})$ represent the Gaussian processes of LF and HF simulation models, respectively, and $Z_d(\mathbf{x})$ represents the difference between $Z_c(\mathbf{x})$ and $Z_e(\mathbf{x})$. The Co-Kriging prediction of the expensive HF simulation model is given by Eq. (9)

$$\hat{y}_e(\mathbf{x}) = \hat{\mu} + \mathbf{c}^T \mathbf{C}^{-1} (\mathbf{y} - \mathbf{1}\hat{\mu})$$

$$\begin{cases} \mathbf{c} = \begin{bmatrix} \hat{\rho} \hat{\sigma}_c^2 \psi_c(\mathbf{X}_c, \mathbf{x}) \\ \hat{\rho}^2 \hat{\sigma}_c^2 \psi_c(\mathbf{X}_c, \mathbf{x}) + \hat{\sigma}_d^2 \psi_d(\mathbf{X}_e, \mathbf{x}) \end{bmatrix} \\ \hat{\mu} = \mathbf{1}^T \mathbf{C}^{-1} \mathbf{Y} / \mathbf{1}^T \mathbf{C}^{-1} \mathbf{1} \end{cases} \quad (9)$$

In Eq. (9), \mathbf{C} is the covariance matrix derived as

$$\mathbf{C} = \begin{bmatrix} \sigma_c^2 \psi_c(\mathbf{X}_c, \mathbf{X}_c) & \rho \sigma_c^2 \psi_c(\mathbf{X}_c, \mathbf{X}_e) \\ \rho \sigma_c^2 \psi_c(\mathbf{X}_c, \mathbf{X}_e) & \rho^2 \sigma_c^2 \psi_c(\mathbf{X}_c, \mathbf{X}_e) + \sigma_d^2 \psi_d(\mathbf{X}_e, \mathbf{X}_e) \end{bmatrix} \quad (10)$$

where $\psi_c(\cdot, \cdot)$ and $\psi_e(\cdot, \cdot)$ represent the correlation matrix between two sets of sample points. The exponential function with hyperparameters θ is used as the correlation function, i.e., $\psi(\mathbf{x}^{(i)}, \mathbf{x}^{(j)}) = \exp(-\sum_{m=1}^{n_v} \theta_m (\mathbf{x}_m^{(i)} - \mathbf{x}_m^{(j)})^2)$ for n_v -dimensional problems.

The maximum likelihood estimations (MLEs) of hyperparameters σ_c^2 and θ_c can be obtained by maximizing Eq. (11) to construct the Kriging metamodel of the cheap simulation model

$$-\frac{n_c}{2} \ln(\hat{\sigma}_c^2) - \frac{1}{2} \ln(|\det(\psi_c(\mathbf{X}_c, \mathbf{X}_c))|)$$

$$\begin{cases} \hat{\mu}_c = \mathbf{1}^T \psi_c(\mathbf{X}_c, \mathbf{X}_c)^{-1} \mathbf{y}_c / \mathbf{1}^T \psi_c(\mathbf{X}_c, \mathbf{X}_c)^{-1} \mathbf{1} \\ \hat{\sigma}_c^2 = (\mathbf{y}_c - \mathbf{1}\hat{\mu}_c)^T \psi_c(\mathbf{X}_c, \mathbf{X}_c)^{-1} (\mathbf{y}_c - \mathbf{1}\hat{\mu}_c) / n_c \end{cases} \quad (11)$$

while the MLEs of hyperparameters ρ , σ_d^2 , and θ_d are the hyperparameters determined by maximizing Eq. (12) to construct the Kriging metamodel of the deviation between the expensive and cheap simulation models, i.e., $\mathbf{d} = \mathbf{Y}_e - \rho \mathbf{y}_c(\mathbf{X}_e)$.

$$-\frac{n_e}{2} \ln(\hat{\sigma}_d^2) - \frac{1}{2} \ln(|\det(\psi_d(\mathbf{X}_e, \mathbf{X}_e))|)$$

$$\begin{cases} \hat{\mu}_d = \mathbf{1}^T \psi_d(\mathbf{X}_e, \mathbf{X}_e)^{-1} \mathbf{d} / \mathbf{1}^T \psi_d(\mathbf{X}_e, \mathbf{X}_e)^{-1} \mathbf{1} \\ \hat{\sigma}_d^2 = (\mathbf{d} - \mathbf{1}\hat{\mu}_d)^T \psi_d(\mathbf{X}_e, \mathbf{X}_e)^{-1} (\mathbf{d} - \mathbf{1}\hat{\mu}_d) / n_e \end{cases} \quad (12)$$

Additionally, the mean-squared error of the Co-Kriging is able to be estimated according to Eq. (13), which is zero at the expensive sample points.

$$s^2(\mathbf{x}) = \hat{\rho} \hat{\sigma}_c^2 + \hat{\sigma}_d^2 - \mathbf{c}^T \mathbf{C}^{-1} \mathbf{c} \quad (13)$$

In fact, Co-Kriging is an interpolator of HF sample points, which integrates the data from LF simulation models to improve the prediction accuracy. More details about the derivation of Co-Kriging can be found in Ref. [21].

4.2 Overall Procedure of the Framework. To efficiently solve the aforementioned all-electric GEO satellite MDO problem with multi-fidelity simulation models, a novel adaptive Co-Kriging-based optimization framework is proposed. In this framework, Co-Kriging metamodels of the objective and constraints are constructed, respectively, based on the samples from HF and LF-MDA processes to represent the expensive simulations for optimization. And the Co-Kriging metamodels are adaptively updated during the optimization via a multi-objective adaptive infill sampling method, which leads the search to the feasible

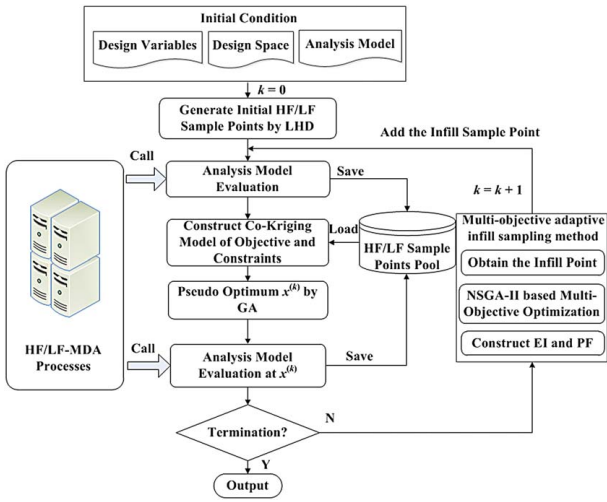


Fig. 9 Flowchart of the adaptive Co-Kriging-based optimization framework

optimum efficiently. The architecture of the framework is displayed in Fig. 9, and the procedures are detailed as follows.

Step 1: The all-electric GEO satellite system multi-fidelity MDO problem and the associated optimization parameters are configured including the multi-fidelity models, number of initial expensive sample points n_{se} , number of initial cheap sample points n_{sc} , and the maximum number of expensive sample points. The iteration count k is set to be 1. In this work, the initial number of LF sample points is calculated by Eq. (14)

$$n_{sc} = \min \{5n_v, (n_v + 1)(n_v + 2)/2\} \quad (14)$$

where n_v is the dimensionality of the optimization problem. The number of HF sample points n_{se} is determined by Eq. (15)

$$n_{se} = \text{round} \left(\frac{\bar{t}(\text{MDA}_{\text{HF}})}{\bar{t}(\text{MDA}_{\text{LF}})} \cdot n_{sc} \right) \quad (15)$$

where $\bar{t}(\text{MDA}_{\text{HF}})$ and $\bar{t}(\text{MDA}_{\text{LF}})$ are the estimated mean time cost of running one trial of HF-MDA and LF-MDA, respectively, and $\text{round}(\cdot)$ represents rounding the value to the nearest integer.

Step 2: Both the initial HF sample points \mathbf{X}_e and LF sample points \mathbf{X}_c are generated by the maximin Latin hypercube design (LHD) method in the design space with $\mathbf{X}_e \subset \mathbf{X}_c$. The associated HF/LF responses including the objective and constraints of the sample points are obtained by evaluating the HF- and LF-MDA processes, respectively.

Step 3: Co-Kriging metamodels of the objective and constraints are, respectively, constructed or updated based on the existing multi-fidelity samples. Then, the Genetic algorithm (GA) is utilized to solve the optimization problem in Eq. (16)

$$\begin{aligned} &\text{find} && \mathbf{X} \\ &\min && \hat{f}(\mathbf{X}) \\ &\text{s.t.} && \mathbf{x}_{\text{LB}} \leq \mathbf{X} \leq \mathbf{x}_{\text{UB}} \\ &&& \hat{g}_i(\mathbf{X}) \leq 0, \quad i = 1, 2, \dots, m \end{aligned} \quad (16)$$

where $\hat{f}(\mathbf{X})$ and $\hat{g}_i(\mathbf{X})$ are Co-Kriging metamodels of the objective and the i th constraint, respectively, \mathbf{x}_{LB} and \mathbf{x}_{UB} are the associated lower and upper bounds of the optimization problem, and $m = 10$ is the number of constraints for the satellite MDO problem. In this paper, GA is configured by the default setting of native MATLAB GA TOOLBOX. The current optimum obtained by GA is referred to as the current pseudo optimum $\mathbf{x}_{\text{opt}}^{(k)}$, which is utilized to determine the infill sample point later. The associated HF and LF objective and

constraints at $\mathbf{x}_{\text{opt}}^{(k)}$ are evaluated and added to both the HF and LF sample pools.

Step 4: If the number of HF-MDA evaluations exceeds the predefined maximum value, the optimization is terminated and the current optimal feasible solution is output; otherwise, the procedure continues.

Step 5: An infill sample point is generated by the proposed multi-objective adaptive infill sampling method to refine the existing Co-Kriging metamodels, which is detailed in Sec. 4.3. Then, set $k = k + 1$, and the procedure turns to *Step 3* to continue the optimization.

4.3 Bi-Objective-Oriented Infill Sampling. Based on the notion of Pareto non-domination set in terms of optimality and feasibility from Ref. [27], a bi-objective-oriented infill sampling approach is developed to effectively produce sequential samples considering feasibility for effectively refining Co-Kriging metamodels and efficiently leading the optimization to the feasible optimum. This novel infill sampling approach is presented in Table 7, and the procedure is detailed as follows.

Step 1 (Line 1): The EI function of the objective is established as shown in Eq. (17) [27]

$$\text{EI} = (f_{\min} - \hat{f}(\mathbf{X}))\Phi \left(\frac{f_{\min} - \hat{f}(\mathbf{X})}{s(\mathbf{X})} \right) + s(\mathbf{X})\phi \left(\frac{f_{\min} - \hat{f}(\mathbf{X})}{s(\mathbf{X})} \right) \quad (17)$$

where $\Phi(\cdot)$ and $\phi(\cdot)$ are the Gaussian cumulative distribution function and probability density function, respectively, and f_{\min} is the minimum objective value of the existing sample points. During the optimization, the EI function needs to be maximized to effectively balance the global exploration and local exploitation performance.

Step 2 (Lines 2–3): The constraint violation function (i.e., $h(\mathbf{X})$) of the MDO problem is formulated by Eq. (18). A positive $h(\mathbf{X})$ represents an infeasible sample point, and a larger $h(\mathbf{X})$ generally indicates worse infeasibility.

$$h(\mathbf{X}) = \max \{g_1(\mathbf{X}), g_2(\mathbf{X}), \dots, g_m(\mathbf{X})\} \quad (18)$$

Based on the existing HF and LF samples, the Co-Kriging metamodel of $h(\mathbf{X})$ is constructed as shown in Eq. (19)

$$\hat{h}(\mathbf{X}) \sim \text{Co-KRG}(\hat{\mu}_h, s_h^2) \quad (19)$$

where $\hat{\mu}_h$ and s_h^2 are the associated hyperparameters of Co-Kriging metamodel for $h(\mathbf{X})$, respectively.

Step 3 (Line 4): Based on $\hat{h}(\mathbf{X})$, the probability of feasibility (PF) function is established as shown in Eq. (20) [27]. The PF function

Table 7 Bi-objective-oriented infill sampling algorithm

Input: Existing HF and LF samples, Co-Kriging metamodels of objective and constraints, design space $\mathbf{V}_0 = [\mathbf{x}_{\text{LB}}, \mathbf{x}_{\text{UB}}]$, current pseudo optimum $\mathbf{x}_{\text{opt}}^{(k)}$

Output: Infill sample point \mathbf{x}^*

Begin

- (1) $\text{EI}(\mathbf{X}) = \text{ConstructEI}(\hat{f}(\mathbf{X}), s(\mathbf{X}), f_{\min})$
- (2) $h(\mathbf{X}) = \max(g_i(\mathbf{X}))$
- (3) $\hat{h}(\mathbf{X}) = \text{Co-Kriging}(\mathbf{X}, h(\mathbf{X}))$
- (4) $\text{PF}(\mathbf{X}) = \text{ConstructPF}(\hat{h}(\mathbf{X}))$
- (5) $\mathbf{X}_{\text{Pareto}} = \text{NSGA-II}(\text{EI}(\mathbf{X}), \text{PF}(\mathbf{X}), \mathbf{V}_0)$
- (6) $\mathbf{X}_{\text{Candidate}} \leftarrow \left[\mathbf{x} \mid \text{EI}(\mathbf{x}) > \text{EI}(\mathbf{x}_{\text{opt}}^{(k)}) \cup \text{PF}(\mathbf{x}) > \text{PF}(\mathbf{x}_{\text{opt}}^{(k)}) \right]$
- (7) $\mathbf{x}^* \leftarrow \max \{ \|\text{EI}(\mathbf{x}), \text{PF}(\mathbf{x}) - (\text{EI}(\mathbf{x}_{\text{opt}}^{(k)}), \text{PF}(\mathbf{x}_{\text{opt}}^{(k)}))\| \}, \mathbf{x} \in \mathbf{X}_{\text{Candidate}}$
- (8) **return** \mathbf{x}^*

End

Table 8 Parameter configuration of NSGA-II

Parameters	NSGA-II
Population size	50
Maximum generations	10
Crossover fraction	0.8
Mutation fraction	0.3
Mutation rate	0.1

represents the probability of $h(\mathbf{X})$ to be less than zero, i.e., the new infill sample is feasible, which should be maximized during the optimization.

$$PF(\mathbf{X}) = \frac{1}{s_h(\mathbf{X})\sqrt{2\pi}} \int_{-\infty}^0 e^{-\frac{(h(\mathbf{X})-\bar{h}(\mathbf{X}))^2}{2s_h^2(\mathbf{X})}} dh(\mathbf{X}) \quad (20)$$

Step 4 (Lines 5–8): The NSGA-II algorithm [28] is utilized to solve the bi-objective optimization problem displayed in Eq. (21). Note that the parameters of NSGA-II can be tuned for different optimization problems in engineering practice. In this paper, NSGA-II is configured by the parameters in Table 8 to balance the algorithm efficiency and the Pareto frontier exploration.

$$\begin{aligned} &\text{find } \mathbf{X} \\ &\max \begin{cases} EI(\mathbf{X}) \\ PF(\mathbf{X}) \end{cases} \\ &\text{s.t. } \mathbf{x}_{LB} \leq \mathbf{X} \leq \mathbf{x}_{UB} \end{aligned} \quad (21)$$

After bi-objective optimization, the Pareto frontier consisting of non-dominated points in terms of EI and PF is obtained. The Pareto frontier points that are not dominated by the current pseudo optimum $\mathbf{x}_{opt}^{(k)}$ are selected as the candidate points. To fully explore the design space and avoid over-crowded points, the candidate point with the largest distance from $\mathbf{x}_{opt}^{(k)}$ is selected as the infill point \mathbf{x}^* , which is graphically expressed in Fig. 10.

4.4 Test on Numerical Benchmarks. Several numerical benchmark problems as listed in Table 9 are utilized to verify the optimization capability of the developed adaptive Co-Kriging method in the aforementioned optimization framework. The formulations of benchmark problems are expressed in the Appendix, which is treated as HF models. In this study, the LF models are

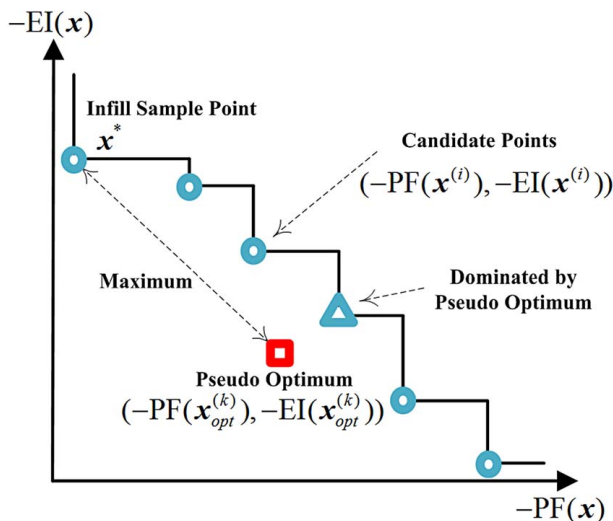


Fig. 10 Illustration of infill sample point determination

Table 9 Information of numerical benchmark problems

Benchmarks	Optimum	Dimensionality	Constraints
G4	-30,665.539	5	6
Hesse	-310.00	6	6
ICE	-55.67	5	9

formulated by directly scaling the associated HF models according to Eq. (22)

$$\begin{aligned} f_{LF}^b &= \eta f_{HF}^b + \delta_f^b \\ g_{LF}^b &= \eta g_{HF}^b + \delta_g^b \end{aligned} \quad (22)$$

where $f_{LF, HF}^b$ and $g_{LF, HF}^b$, respectively, represent the objective and constraint responses from the LF/HF models, $\eta=0.9$ is the scaling factor, and $\delta_f^b = 0.5$ and $\delta_g^b = -0.05$ are the predefined constant deviations.

For comparison, the well-known EGO algorithm [12] is also utilized to solve the benchmark problems. In EGO, the original Kriging metamodel is replaced by Co-Kriging for multi-fidelity optimization. At each EGO iteration, the infill HF and LF samples are allocated via maximizing the constrained expected improvement [29] as shown in Eq. (23)

$$CEI(\mathbf{X}) = EI(\mathbf{X}) \cdot \prod_{i=1}^m PF_i(\mathbf{X}) \quad (23)$$

where $PF_i(\mathbf{X})$ is the PF function of the i th constraint.

In the benchmark tests, the number of initial LF and HF sample points are determined by Eqs. (14) and (15), where $\bar{i}(MDA_{LF})$ is assumed to be half of $\bar{i}(MDA_{HF})$. For both methods, the maximum number of HF sample points is set to be 30. Considering the stochastic behavior in the proposed optimization framework caused by GA search and LHD sampling, each benchmark test is consecutively performed by ten trials. The obtained best feasible solutions in ten trials are graphically expressed in Fig. 11. The median/mean values of objectives and the number of used HF/LF sample points are summarized in Table 10. Since the proposed method and competitive EGO consume the same computational cost for all the benchmark problems, we mainly focuses on discussing their convergence performance.

The lowest values of best feasible solutions in Fig. 11 indicate that the proposed adaptive Co-Kriging method can successfully find the theoretical optima for all the benchmark problems. Meanwhile, EGO only converges to the vicinity of global optima with the same number of sample points. Figure 11 also exhibits that the variations of adaptive Co-Kriging method is much smaller than those of EGO. In terms of the mean and median values of

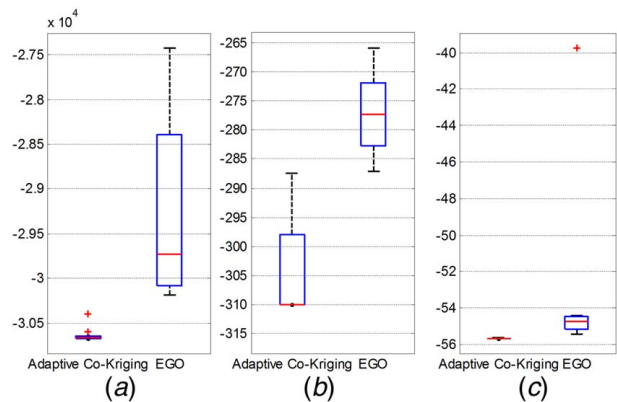


Fig. 11 Comparison of best feasible solutions in ten trials: (a) G4, (b) Hesse, and (c) ICE

Table 10 Optimization results for different benchmarks

		G4	Hesse	ICE
Adaptive Co-Kriging	Median	-30,664.760	-309.97	-55.67
	Mean	-30,633.096	-303.34	-55.67
	HF samples	30	30	30
	LF samples	42	44	42
EGO	Median	-29,730.880	-277.34	-54.74
	Mean	-29,290.080	-276.80	-53.35
	HF samples	30	30	30
	LF samples	42	44	42

feasible solutions, the proposed adaptive Co-Kriging method also outperforms the competitive EGO as shown in Table 10. In summary, the proposed adaptive Co-Kriging method generally shows better global convergence than the conventional EGO with the same computational budget, which is highly promising for solving the all-electric GEO satellite MDO problem.

5 Optimization and Discussion

In this section, the adaptive Co-Kriging-based optimization framework is employed to effectively solve the aforementioned all-electric GEO satellite MDO problem with multi-fidelity models. The optimization results are detailed to demonstrate the merits of the proposed optimization framework.

5.1 Optimization Results. In the adaptive Co-Kriging-based optimization framework, the number of initial LF sample points is set to be 75, i.e., $n_v = 15$ according to Eq. (14). The number of initial HF sample points is set as 38 according to Eq. (15) and Table 6. The maximum number of HF sample points is set to be 100 to balance the efficiency and convergence of optimization. The maximum constraint violation tolerance for the satellite MDO problem is set to be 0.05 [8].

In this work, a baseline design of the satellite is derived from Ref. [8]. The optimized design from the proposed adaptive Co-Kriging-based optimization framework and the baseline design are listed in Table 11, while the associated constraints are summarized in Table 12. The iteration history of the objective (i.e., the total mass of the satellite system) and maximum constraint violation during the optimization are graphically illustrated in Fig. 12. And the objective of the optimized design is compared with that of the baseline design in Table 13.

From Table 12, the empirical baseline design is infeasible because the total transfer time constraint is not satisfied; on the contrary, all of the constraints are satisfied in the optimized design. Some constraints (i.e., EWSK accuracy, ending-of-life power, depth of discharge) reach the associated bounds values and become active, which indicates the optimality of the solution. Figure 12 illustrates that the objective is consistently improved during the optimization process, while the constraint violation is strictly limited within the predefined tolerances. As shown in Table 11, the yaw angle in the first stage of GTO is decreased to zero after optimization, which improves the efficiency of orbit raising and therefore reduces the transfer time. The low-thrust transfer trajectory of the optimized design is illustrated in Fig. 13. Besides making the design feasible, the Co-Kriging-based multi-fidelity optimization also yields a 156.3 kg decrease in total mass, i.e., 5.85% of the entire satellite system, as shown in Table 13. To reduce the mass, the area of solar arrays and capacity of the battery in the optimized design are also decreased by 4.8% and 7.9%, respectively, according to Table 11. Additionally, the thickness of the structure plates and bearing cylinder is also decreased while the natural frequencies constraints are still satisfied, whose modal shapes are illustrated in Fig. 14. Owing to the reduced size of solar arrays and buffer mass of subsystems, the needed angular momentum of reaction wheel is only 74.3% of that in the initial design, and the area of radiators is also decreased by 13.8%, which further reduces the entire system mass.

5.2 Discussions. To further illustrate the merits of adaptive Co-Kriging-based multi-fidelity optimization for all-electric GEO satellite MDO problem, our previously published sequential radial basis function using support vector machine (SRBF-SVM) [17] and adaptive response surface method with intelligent space exploration strategy (ARSM-ISES) [30] are also utilized to optimize the satellite system for comparison.

SRBF-SVM constructs the radial basis function (RBF) metamodels of expensive objective and constraints for optimization. And the RBF metamodels are adaptively refined via sequentially sampling in a promising sub-region identified by support vector machine. SRBF-SVM has been proved to be quite effective for solving expensive black-box optimizations and successfully been applied to a small Earth observation satellite MDO problem [17]. ARSM-ISES approximates expensive simulations by a second-order response surface model (RSM) for optimization. An intelligent space exploration strategy is developed for updating RSM to improve efficiency and global convergence performances.

Table 11 Comparison of baseline design and optimized design

Design variable	Symbol	Unit	Bounds	Baseline design	Optimized design
Yaw angle in the first stage of GTO	α	deg	[0,45]	30	0.0
Pitch angle in the first stage of GTO	β	deg	[0,45]	30	34.7
Pitch angle in the second stage of GTO	φ	deg	[30,45]	30	38.8
The T position of the thruster	d_T	mm	[500,1180]	900	500.0
The N position of the thruster	d_N	mm	[800,1050]	900	1050.0
Area of solar arrays	A_{sa}	m ²	[60,90]	80	76.2
Capacity of battery	C_s	Ah	[60,90]	80	73.7
Area of radiators	A_r	m ²	[5,10]	8	6.9
Angular momentum of reaction wheel	H_w	N m s	[25,50]	40	29.7
Core thickness of service cabin plates	SH	mm	[15,25]	20	15.0
Core thickness of communication cabin plates	CH	mm	[15,25]	20	15.0
Core thickness of central cylinder	TBH	mm	[15,25]	25	18.1
Ply thickness of service cabin plates	SP	mm	[0.1,0.2]	0.15	0.10
Ply thickness of communication cabin plates	CSP	mm	[0.1,0.2]	0.15	0.10
Ply thickness of bearing cylinder	TBP	mm	[0.1,0.2]	0.2	0.15

Table 12 Constraint values of the initial design and optimized design

Constraint	Symbol	Unit	Range	Baseline design	Optimized design
Total orbit transfer time	t_f	day	≤ 214	231.5	198.7
EWSK accuracy	λ_{\max}	deg	≤ 0.05	0.05	0.05
NSSK accuracy	i_{\max}	deg	≤ 0.05	0.01	0.01
Beginning-of-life power	P_{BOL}	kW	≥ 14.15	15.05	14.66
Ending-of-life power	P_{EOL}	kW	≥ 11.90	12.18	11.90
Depth of discharge	DOD	-	≤ 0.8	0.74	0.80
Steady-state temperature	T	K	[267,328]	317.5	327.7
Angular momentum residue	c_{AC}	N m s	≥ 0	0.95	0.23
First rotational modal frequency round X-axis	f_X	Hz	≥ 5	5.69	5.2
First rotational modal frequency round Y-axis	f_Y	Hz	≥ 5	5.75	5.3

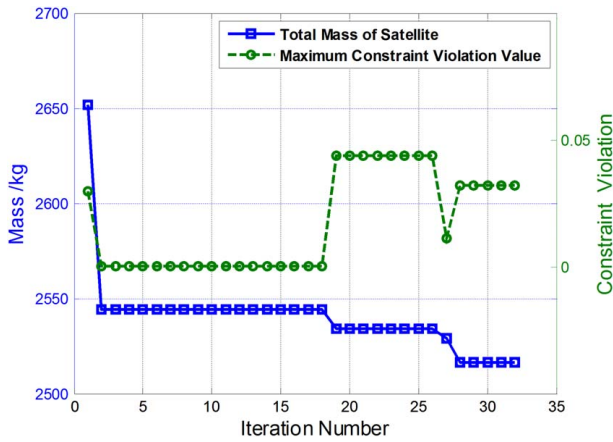


Fig. 12 History curves of objective and maximum constraint violation

Table 13 Comparison of the optimized system mass

Index	Baseline design	Optimized design
Total mass	2672.8	2516.5 kg

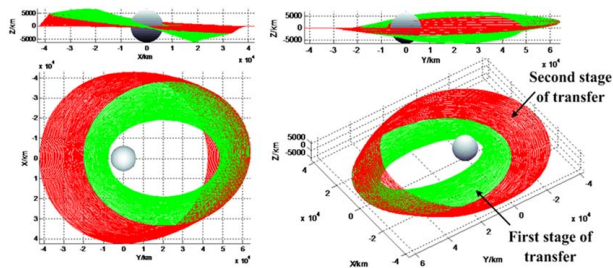


Fig. 13 Optimized trajectory of the transfer orbit

ARSM-ISES has also been successfully applied to solve the all-electric GEO satellite MDO problem with single-fidelity models in Ref. [8].

To prove the significance of multi-fidelity optimization, both SRBF-SVM and ARSM-ISES are applied to solve the all-electric GEO satellite MDO problem with high-fidelity models alone in this paper. The maximum number of HF sample points for SRBF-SVM is set to be 237, i.e., the total number of sample points for the multi-fidelity optimization in Sec. 5.1. ARSM-ISES

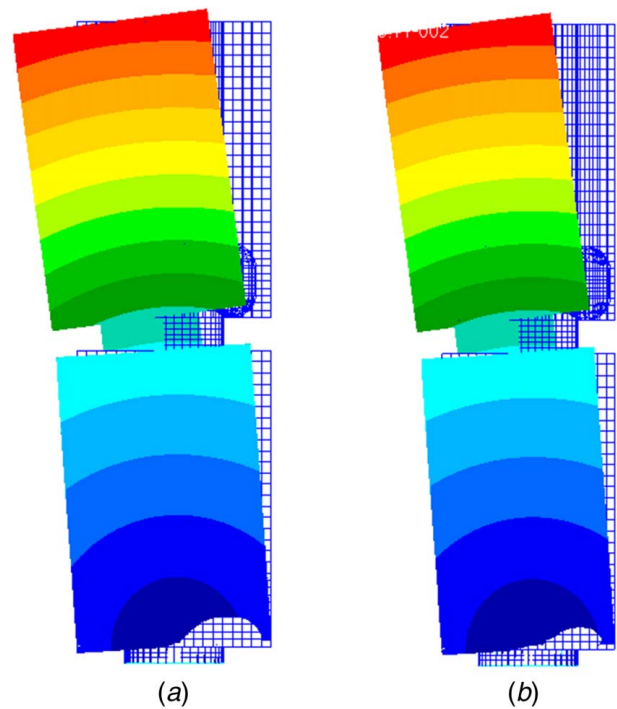


Fig. 14 Modal shapes of the optimized structure: (a) around X-axis and (b) around Y-axis

follows the same configuration in Ref. [8]. The optimization results of SRBF-SVM and ARSM-ISES are briefly summarized in Table 14. The optimized objectives and computational costs consumed for optimization are compared in Table 15.

As shown in Table 14, both SRBF-SVM and ARSM-ISES can successfully find a feasible solution of the all-electric GEO satellite MDO problem by purely using HF models. But the optimized total mass from adaptive Co-Kriging optimization is 97.6 kg and 36.8 kg lower than that of SRBF-SVM and ARSM-ISES, respectively. Moreover, owing to using cheap LF samples, the computational cost of adaptive Co-Kriging-based multi-fidelity optimization is significantly reduced by 40% and 82%, respectively, than that of SRBF-SVM and ARSM-ISES with pure HF samples. This efficiency merit of multi-fidelity optimization is desirable in spacecraft system design practices when the computational cost is limited.

From the optimization results and discussions above, the proposed adaptive Co-Kriging-based optimization framework is feasible and effective to solve the all-electric GEO satellite multi-fidelity MDO problems with multi-fidelity models. Via multi-fidelity

Table 14 Optimization results of competitive algorithms

		SRBF-SVM	ARSM-ISES
Design variables	α/deg	18.1	7.12
	β/deg	29.2	27.69
	φ/deg	35.6	44.21
	d_T/mm	517.2	614.22
	d_N/mm	886.6	824.93
	A_{s0}/m^2	79.2	75.98
	C_s/Ah	81.7	73.66
	A_p/m^2	8.1	8.72
	$H_w/\text{N m s}$	41.3	45.67
	SH/mm	15.7	24.14
	CH/mm	18.4	15.04
	TBH/mm	18.7	16.97
	SP/mm	0.14	0.105
	CSP/mm	0.11	0.102
	TBP/mm	0.15	0.161
	Constraints	t/day	213.3
$\lambda_{\max}/\text{deg}$		0.04	0.04
i_{\max}/deg		0.01	0.01
P_{BOL}/kW		15.10	14.69
P_{EOL}/kW		12.23	11.90
DOD		0.72	0.80
T/K		316.8	308.42
$c_{AC}/\text{N m s}$		10.3	16.23
f_x/Hz		5.2	5.35
f_y/Hz		5.2	5.41

Table 15 Optimization results of competitive algorithms

	SRBF-SVM	ARSM-ISES	Adaptive Co-Kriging
Total mass	2614.1 kg	2553.3 kg	2516.5 kg
HF samples	237	817	100
LF samples	None	None	137
Running time	~15 h	~50 h	~9 h

optimization, the total mass of the satellite system can be significantly reduced to save the launch and deployment cost, which improves the overall performance of the system and produces considerable economic benefits from the customers' perspective. Additionally, comparing with the state-of-art metamodel-based optimization with HF models alone, the adaptive Co-Kriging-based multi-fidelity optimization can significantly reduce the computational cost. The investigations demonstrate the effectiveness and practicality of the multi-fidelity modeling and adaptive Co-Kriging-based optimization work in this paper for all-electric GEO satellite system design practices.

6 Conclusions

In this paper, an all-electric GEO satellite MDO problem with multi-fidelity models is investigated. The analysis models of GTO and structures with different levels of fidelity are developed to perform the multi-fidelity multidisciplinary optimization. As for the GTO discipline, a two-stage strategy is utilized to implement the low-thrust GEO transfer, where the dynamics formulation and simulation step are taken into account to construct different fidelity models. As for the structure, the HF model is built as an adjoined double-satellite FEA simulation, while the LF model is tuned from an isolated satellite FEA simulation. Given the multi-fidelity models, a novel adaptive Co-Kriging-based optimization framework is proposed to effectively solve the satellite MDO problem. In this framework, the Co-Kriging metamodels of objective and constraints are constructed for optimization based on the limited samples arising from HF- and LF-MDA processes. During the optimization, the Co-Kriging metamodels are gradually updated via the

multi-objective adaptive infill sampling approach. In this approach, the EI and PF functions of the objective are, respectively, constructed based on the associated Co-Kriging metamodel. And the NSGA-II algorithm is utilized to simultaneously optimize the EI and PF functions to obtain a set of Pareto frontier points, where the infill point is determined by the information of current pseudo optimum. Several numerical benchmark problems are tested to demonstrate the effectiveness of the framework. Finally, the proposed optimization framework is applied to solve the all-electric GEO satellite multi-fidelity MDO problem. The results show that the total mass of satellite system is decreased by 156.3 kg, which is a remarkable improvement for the overall system performance. Additionally, owing to the efficiency of multi-fidelity modeling, the computational cost is significantly reduced compared with our previous proposed SRBF-SVM and ARSM-ISES which purely uses HF models for optimization.

In future work, more disciplinary models with different levels of fidelity are expected to be integrated within the MDO problem to further improve the design quality and reduce the optimization cost for all-electric GEO satellite systems. Since the error margin in LF models can significantly affect the approximation accuracy of Co-Kriging, the influences of error margin will be investigated to further enhance the optimization capability of the proposed optimization framework. Note that the adaptive Co-Kriging-based optimization framework in this paper is also applicable to the multi-fidelity optimization of other sophisticated systems (e.g., automobile, aircraft), more engineering applications are expected to be investigated in the future.

Acknowledgment

This work was supported by the National Natural Science Foundation of China (Grant No. 51675047, 11372036; Funder ID: 10.13039/501100001809), Aeronautic Science Foundation of China (Grant No. 2015ZA72004; Funder ID: 10.13039/501100004750), International Cooperation Program Fund of Beijing Institute of Technology (Grant No. GZ2018015101; Funder ID: 10.13039/501100010896), and Natural Science and Engineering Research Council (NSERC) of Canada (Grant No. R611512 WANG, G-RGPIN04291; Funder ID: 10.13039/501100000038). The leading author also would like to appreciate the China Scholarship Council (CSC) to financially support his study in SFU (Grant No. 201706030009; Funder ID: 10.13039/501100004543).

Appendix

Disciplinary Coupled Relationships. The coupled state variables in the DSM as shown in Fig. 1 are defined in Table 16 [8].

Table 16 Definitions of coupled state variables

Symbol	Definition
y_{12}	Initial satellite mass in GEO
y_{13}	Transfer information and flying time during the radiation belt, power requirement of the satellite in GTO
y_{14}	Extreme external heat flux
y_{15}	Transfer information
y_{16}	Mass of fuel used in GTO
y_{23}	Power requirement in GEO operation
y_{26}	Mass of fuel used in GEO position keeping
y_{34}	Output power of solar arrays
y_{35}	Area of solar arrays
y_{36}	Mass of power subsystem
y_{46}	Mass of thermal control subsystem
y_{56}	Mass of attitude control subsystem
y_{61}	Total mass of the satellite, objective
y_{62}	Center of gravity height
y_{64}	Total mass of satellite, objective
y_{65}	Moments of inertia

Numerical Benchmark Problems. The formulations of the numerical benchmark problems are presented as follows: ICE [31]:

$$\begin{aligned}
 \max f(x) &= K_0((\rho Q/A_f)\eta_t\eta_v - FMEP), \quad x = [b, c_r, d_E, d_I, w] \\
 70 \leq b \leq 90, 6 \leq c_r \leq 10, 30 \leq d_E \leq 40, 35 \leq d_I \leq 45, 4 \leq w \leq 8 \\
 \eta_v &= \eta_{vb}[1 + 5.96 \times 10^{-3}w^2]/[1 + [(9.428 \times 10^{-5}) \\
 &\quad \times (4V/\pi N_c C_s)(w/d_I^2)]^2] \\
 \eta_{vb} &= \begin{cases} 1.067 - 0.038 \exp(w - 5.25), & (w \geq 5.25) \\ 0.637 + 0.13w - 0.014w^2 + 0.00066w^3, & (w \leq 5.25) \end{cases} \\
 \eta_{tad} &= 0.8595(1 - c_r^{-0.33}) \\
 \eta_t &= \eta_{tad} - S_v(1.5/w)^{0.5} \\
 S_v &= (0.83)[(8 + 4c_r) + 1.5(c_r - 1)(\pi N_c/V)b^3]/[(2 + c_r)b] \\
 FMEP &= (4.826)(c_r - 9.2) + (7.97 + 0.253V_p + 9.7(10^{-6})V_p^2) \\
 V_p &= (8V/\pi N_c)wb^{-2} \\
 \text{s.t.} \\
 g_1 &= K_1N_cb - L_1 \leq 0 \\
 g_2 &= (4K_2V/\pi N_cL_2)^{1/2} - b \leq 0 \\
 g_3 &= d_I + d_E - K_3b \leq 0 \\
 g_4 &= K_4d_I - d_E \leq 0 \\
 g_5 &= d_E - K_5d_I \leq 0 \\
 g_6 &= (9.428)(10^{-5})(4V/\pi N_c)(w/d_I^2) - K_6C_s \leq 0 \\
 g_7 &= c_r - 13.2 + 0.045b \leq 0 \\
 g_8 &= w - K_7 \leq 0 \\
 g_9 &= 3.6(10^6) - K_8Q\eta_{tw} \leq 0 \\
 \eta_{tw} &= 0.8595(1 - c_r^{-0.33}) - S_v
 \end{aligned} \tag{A1}$$

Hesse [14]:

$$\begin{aligned}
 f(x) &= -25(x_1 - 2)^2 - (x_2 - 2)^2 - (x_3 - 1)^2 - (x_4 - 4)^2 - (x_5 - 1)^2 - (x_6 - 4)^2 \\
 0 \leq x_1 \leq 5, 0 \leq x_2 \leq 4, 1 \leq x_3 \leq 5, 0 \leq x_4 \leq 6, 1 \leq x_5 \leq 5, 0 \leq x_6 \leq 10 \\
 \text{s.t.} \\
 g_1(x) &= (2 - x_1 - x_2)/2 \leq 0 \\
 g_2(x) &= (x_1 + x_2 - 6)/6 \leq 0 \\
 g_3(x) &= (-x_1 + x_2 - 2)/2 \leq 0 \\
 g_4(x) &= (x_1 - 3x_2 - 2)/2 \leq 0 \\
 g_5(x) &= (4 - (x_3 - 3)^2 - x_4)/4 \leq 0 \\
 g_6(x) &= (4 - (x_5 - 3)^2 - x_6)/4 \leq 0
 \end{aligned} \tag{A2}$$

G4 [14]:

$$\begin{aligned}
 f(x) &= 5.3578547x_3^2 + 0.8356891x_1x_5 + 37.293239x_1 - 40792.141 \\
 78 \leq x_1 \leq 102, 33 \leq x_2 \leq 45, 27 \leq x_i \leq 45, i = 3, 4, 5 \\
 \text{s.t.} \\
 u &= 85.334407 + 0.0056858x_2x_5 + 0.0006262x_1x_4 - 0.0022053x_3x_5 \\
 g_1(x) &= -u \leq 0 \\
 g_2(x) &= u - 92 \leq 0 \\
 v &= 80.51249 + 0.0071317x_2x_5 + 0.0029955x_1x_2 + 0.0021813x_3^2 \\
 g_3(x) &= -v + 90 \leq 0 \\
 g_4(x) &= v - 110 \leq 0 \\
 w &= 9.300961 + 0.0047026x_3x_5 + 0.0012547x_1x_3 + 0.0019085x_3x_4 \\
 g_5(x) &= -w + 20 \leq 0 \\
 g_6(x) &= w - 25 \leq 0
 \end{aligned} \tag{A3}$$

References

- [1] Boeing Defense, 2018, Space & Security, 702SP Spacecraft, http://www.boeing.com/resources/boeingdotcom/space/boeing_satellite_family/pdf/Bkgd_702SP.pdf, Accessed July 31, 2019.
- [2] Dutta, A., Libraro, P., Kasdin, N. J., Choueiri, E., and Francken, P., 2013, "Design of Next Generation all-Electric Telecommunication Satellites," AIAA International Communication Satellite Systems Conference, Florence, Italy, Oct. 14–17, pp. 5625–5635.
- [3] Dutta, A., Kasdin, N. J., Choueiri, E., and Francken, P., 2016, "Minimizing Proton Displacement Damage Dose During Electric Orbit Raising of Satellites," *J. Guid. Control Dynam.*, **39**(4), pp. 960–966.
- [4] Sobieski, I., 1993, "Multidisciplinary Design Optimization: Attempt at Definition," Industry University Workshop on Multidisciplinary Aircraft Design, Blacksburg, VA, pp. 23–48.
- [5] Castellini, F., Lavagna, M. R., Riccardi, A., and Büskens, C., 2013, "Quantitative Assessment of Multidisciplinary Design Models for Expendable Launch Vehicles," *J. Spacecr. Rockets*, **51**(1), pp. 343–359.
- [6] Hwang, J. T., Lee, D. Y., Cutler, J. W., and Martins, J. R., 2014, "Large-Scale Multidisciplinary Optimization of a Small Satellite's Design and Operation," *J. Spacecr. Rockets*, **51**(5), pp. 1648–1663.
- [7] Huang, H., An, H., Wu, W., Zhang, L., Wu, B., and Li, W., 2014, "Multidisciplinary Design Modeling and Optimization for Satellite With Maneuver Capability," *Struct. Multidiscip. Optim.*, **50**(5), pp. 883–898.
- [8] Shi, R., Liu, L., Long, T., Liu, J., and Yuan, B., 2017, "Surrogate Assisted Multidisciplinary Design Optimization for an All-Electric GEO Satellite," *Acta Astronaut.*, **138**(2017), pp. 301–317.
- [9] Wang, G. G., and Shan, S., 2007, "Review of Metamodeling Techniques In Support of Engineering Design Optimization," *ASME J. Mech. Des.*, **129**(4), pp. 370–380.
- [10] Forrester, A. I. J., and Keane, A. J., 2009, "Recent Advances in Surrogate-Based Optimization," *Prog. Aerosp. Sci.*, **45**(1–3), pp. 50–79.
- [11] Queipo, N. V., Haftka, R. T., Shyya, W., Goela, T., Vaidyanathana, R., and Tucker, P. K., 2005, "Surrogate-Based Analysis and Optimization," *Prog. Aerosp. Sci.*, **41**(1), pp. 1–28.
- [12] Jones, D. R., Schonlau, M., and Welch, W. J., 1998, "Efficient Global Optimization of Expensive Black-Box Functions," *J. Global Optim.*, **13**(4), pp. 455–492.
- [13] Regis, R. G., and Shoemaker, C. A., 2013, "Combining Radial Basis Function Surrogates and Dynamic Coordinate Search in High-Dimensional Expensive Black-Box Optimization," *Eng. Optim.*, **45**(5), pp. 529–555.
- [14] Regis, R. G., 2014, "Constrained Optimization by Radial Basis Function Interpolation for High-Dimensional Expensive Black-Box Problems with Infeasible Initial Points," *Eng. Optim.*, **46**(2), pp. 218–243.
- [15] Müller, J., and Woodbury, J. D., 2017, "GOSAC: Global Optimization With Surrogate Approximation of Constraints," *J. Global Optim.*, **69**(2017), pp. 117–136.
- [16] Peng, L., Liu, L., Long, T., and Yang, W., 2014, "An Efficient Truss Structure Optimization Framework Based on CAD/CAE Integration and Sequential Radial Basis Function Metamodel," *Struct. Multidiscip. Optim.*, **50**(2), pp. 329–346.
- [17] Shi, R., Liu, L., Long, T., and Liu, J., 2016, "Sequential Radial Basis Function Using Support Vector Machine for Expensive Design Optimization," *AIAA J.*, **55**(1), pp. 214–227.
- [18] Chen, S., Jiang, Z., Yang, S., and Chen, W., 2016, "Multimodel Fusion Based Sequential Optimization," *AIAA J.*, **55**(1), pp. 241–254.
- [19] Viana, F. A., Simpson, T. W., Balabanov, V., and Toropov, V., 2014, "Special Section on Multidisciplinary Design Optimization: Metamodeling in Multidisciplinary Design Optimization: How Far Have We Really Come?," *AIAA J.*, **52**(4), pp. 670–690.
- [20] Qian, Z., Seepersad, C. C., Joseph, V. R., Allen, J. K., and Wu, C. J., 2006, "Building Surrogate Models Based on Detailed and Approximate Simulations," *ASME J. Mech. Des.*, **128**(4), pp. 668–677.
- [21] Forrester, A. I. J., Söbester, A., and Keane, A. J., 2007, "Multi-fidelity Optimization via Surrogate Modelling," *Proc. R. Soc. A*, **463**(2088), pp. 3251–3269.
- [22] Ye, H., Clemens, M., and Seifert, J., 2015, "Dimension Reduction for the Design Optimization of Large Scale High Voltage Devices Using Co-Kriging Surrogate Modeling," *IEEE Trans. Magn.*, **51**(3), pp. 1–4.
- [23] Xiong, Y., Chen, W., and Tsui, K. L., 2008, "A new Variable-Fidelity Optimization Framework Based on Model Fusion and Objective-Oriented Sequential Sampling," *ASME J. Mech. Des.*, **130**(11), pp. 699–708.
- [24] Ma, X., Han, D., and Tang, L., 2015, "On the Electric-Propulsion-Based Geostationary Transfer and Space Environmental Analysis," *Aerosp. Control Appl.*, **41**(1), pp. 31–35.
- [25] Ghosh, A., and Coverstone, V., 2015, "Optimal Cooperative CubeSat Maneuvers Obtained Through Parallel Computing," *Acta Astronaut.*, **107**, pp. 130–149.
- [26] Yang, J., 2001, *Spacecraft Orbit Dynamics and Control*, China Astronautic Publishing House, Beijing.
- [27] Parr, J. M., Keane, A. J., Forrester, A. I., and Holden, C. M. E., 2012, "Infill Sampling Criteria for Surrogate-Based Optimization With Constraint Handling," *Eng. Optim.*, **44**(10), pp. 1147–1166.
- [28] Deb, K., Pratap, A., Agarwal, S., and Meyarivan, T. A. M. T., 2002, "A Fast and Elitist Multiobjective Genetic Algorithm: NSGA-II," *IEEE Trans. Evol. Comput.*, **6**(2), pp. 182–197.
- [29] Forrester, A., and Keane, A., 2008, *Engineering Design Via Surrogate Modelling: A Practical Guide*, John Wiley & Sons, Hoboken, NJ.
- [30] Long, T., Wu, D., Guo, X., Wang, G. G., and Liu, L., 2015, "Efficient Adaptive Response Surface Method Using Intelligent Space Exploration Strategy," *Struct. Multidiscip. Optim.*, **51**(6), pp. 1335–1362.
- [31] Gano, S. E., Renaud, J. E., Martin, J. D., and Simpson, T. W., 2006, "Update Strategies for Kriging Models Used in Variable Fidelity Optimization," *Struct. Multidiscip. Optim.*, **32**(4), pp. 287–298.